WOOD RESEARCH doi.org/10.37763/wr.1336-4561/66.5.806820
e-ISSN 2729-8906
66(5): 2021 806-820 pp.

MODELLING OF STEEL-TIMBER COMPOSITE BEAMS: VALIDATION OF FINITE ELEMENT MODEL AND PARAMETRIC STUDY

RUYUAN YANG[1], JIA WAN[2], XIAOFENG ZHANG[3], YOUFU SUN[3]

[1]NANJING TECH UNIVERSITY, CHINA
[2]TAIYUAN UNIVERSITY OF TECHNOLOGY, CHINA
[3]NANJING FORESTRY UNIVERSITY, CHINA

(RECEIVED DECEMBER 2020)

ABSTRACT

In this paper, non-linear finite elements models (FEM) of steel-timber composite (STC) beams have been developed and analyzed using ABAQUS software. In the FEM, the loading conditions of STC beams were simulated, and the nonlinear behaviour of the contact interface between the steel and timber components were incorporated adequately into the FEM. For the yield load, the maximum error between the FE results and the experimental results is 14.85%. The maximum average error of the yield deflection is 12.94%. and of the ultimate load is 16.79%. However, the error of key points was less than 17% (within a reasonable range), which proves that the established finite element model, selected material parameters and contact element model can better simulate the bending performance of STC beams. Finally, a parametric study was carried out by using the verified FEM. It is shown that the FEM developed in this study can replicate adequately the load-deflection response, and the development of stress and plasticity of the bending experiment. Through the parameter study, it can be seen that the distribution density and mechanical properties of the connection between the glulam and H-section steel can affect the mechanical behavior of the whole STC beams.

KEYWORDS: Finite element model (FEM), steel-timber composite, load-deflection response, non-linearity, parametric study.

INTRODUCTION

In order to expand the application of timber structure, in recent years, numerous research projects have been conducted and are currently ongoing to find ways for its wider application in construction through "engineering" of the basic material (Li et al. 2017, 2020). Moreover, timber is also combined with other materials to improve its bearing capacity, such as timber-concrete

composite (TCC) (Schänzlin and Fragiacomo 2017, Daňková et al. 2019, Naud et al. 2019) and other mechanically jointed structures (Yeoh et al. 2011, Khorsandnia et al. 2012, Deam et al. 2008). These composite materials exploit beneficial effects of different materials in different orientations and work as efficient building components in various types of applications. Many researchers reported wide range of numerical analysis and experimental research on the structural performance both short-term and long-term performance of composite materials during the past decades (Fojtik et al. 2020, Yang et al. 2020, Pulngern et al. 2020). Connection and construction methods of composite structure have also been reported by various researchers (Jorge et al. 2011, Leborgne and Gutkowski 2010). In western countries, composite structure has been widely used for its excellent structural performance.

Although there have been a lot of experimental and theoretical studies on the structural performance of composite members with TCC, application on steel-timber composite structure (STC) has not been thoroughly explored in the past. Steel structure offers high strength with a number of beneficial properties but thin-walled steel sections are vulnerable to instability due to buckling. The combination of H-Section steel and glulam by shear connectors can exploit the compressive resistance of timber and can prevent premature failure of the H-section due to torsion and buckling when used as girders. In comparison to bare steel members, STC members have improved stability and bearing capacity, high degree of assembly and low cost of construction and maintenance, which eventually have a relatively positive impact on the environment.

The finite element (FE) numerical simulation is the supplement and extension of the structural experiment. Xu et al. (2015) studied the mechanical performance of steel beam-glulam column composite members through cyclic test and nonlinear finite element (FE) simulations. Liu et al. (2016) developed a three-dimensional (3D) FEM to investigate the structural behaviour of steel-concrete composite beams with Ultra-High Performance Fiber Reinforced Concrete (HSFGB) shear connectors, the accuracy and reliability of the proposed finite element model are validated by comparing their results with available experimental results. Hassanieh et al. (2016, 2017, 2018) investigated the mechanical behaviour of STC connections and beams using a 3D continuum-based FEM, then FEM were validated by experimental tests. It was shown that the FEM can replicate adequately the mechanical behaviour of STC structures tested. Nouri et al. (2019) carried out experimental study on steel-timber composite (STC) beam-to-column connections with double web angles, and nonlinear 3D continuum-based FE simulations were employed to investigate the structural behaviour of this connection.

In current study, the commercial FEM software ABAQUS was used to establish and analyze the 3D FEM of the STC beams, simulate the loading conditions, adopt the reasonable material model and constitutive laws, and simulate the connection mode of H-section steel and glulam. The accuracy and reliability of the proposed FE model were validated by comparing their results with available experimental results. Finally, a parametric study was presented to the flexural behavior of STC beams, and the effects of different types and spacing of shear connectors on the yield load, yield deflection and ultimate bearing capacity of STC beams were considered.

MATERIAL AND METHODS

Outline of four-point bending tests

Fig. 1 shows the sectional dimensions and processing diagram of the STC beam used to verify the FEM. Timber specimen used in the current study was *Larix gmelinii* with lumber dimensions of 3000 × 200 × 40 mm (length × width × height) as the raw material, with a moisture content of 9-12% after drying.

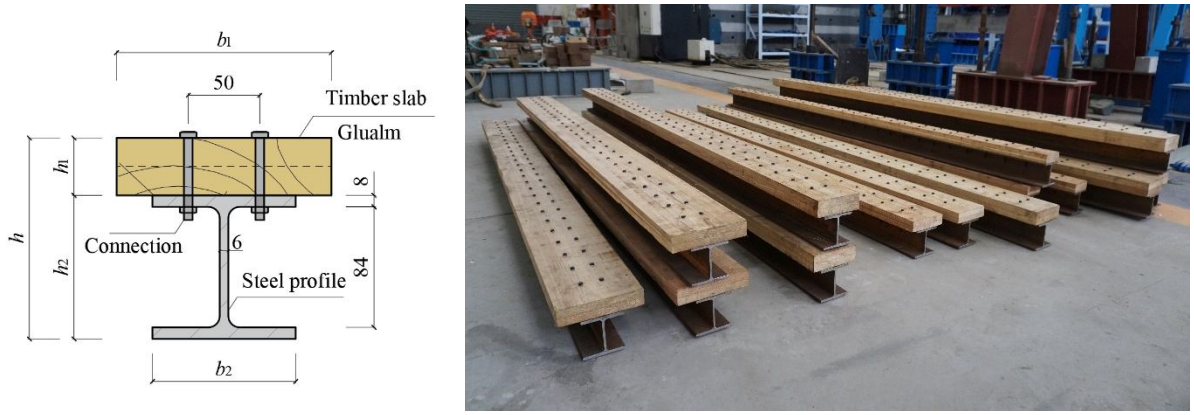

(a) (b)

Fig. 1: Configuration of specimens used in test (all dimensions are in mm): (a) sectional dimensions, (b) perspective view.

Material test was conducted on the raw material following ASTM D143-14: 2014 and basic material properties are shown in Tab. 1. In reference to ANSI A190.1: 2012, glulam slabs consisting of two layers were prepared. Phenol-resorcinol- formaldehyde resin adhesive was used, with a single-side spreading rate of 300 g·m^{-2}, gluing pressure of 1 MPa, lamination time of 3 hours, and curing time of 6 hours. Tests were commenced 7 days after curing.

Tab.1: Basic properties of Larix gmelinii.

Stress direction	f_u (MPa)	μ_{LT}	E (GPa)
Parallel-to-grain compression	50.62	0.3263	13.716
Parallel-to-grain tensile	117.10	0.3214	14.014
Parallel-to-grain shear	9.50	-	-

Note: f_u - ultimate strength (MPa); μ_{LT} - Poisson's ratio of material; and E - elastic modulus (GPa).

Steel profile used in the current research was a hot-rolled steel H-section, which meets relevant standards of GB 50017: 2017 and GB/T50011: 2016 (HW100 × 100 of grade Q235). The thickness of the flange is 8 mm, and that of the web is 6 mm. Laser pilot holes were drilled at relevant positions of the H-section flange and timber, and H-section and glulam holes were accurately aligned (opening diameter 7 mm). The spacing between holes along the span direction was 100 mm, and in transverse direction the spacing was 50 mm. Material test was conducted following ASTM A370-16 (ASTM A370 2016) and basic material properties are shown in Tab. 2.

Tab. 2: Mechanical properties of H steel beam.

f_y (MPa)	f_t (MPa)	f_t/f_y	**Poisson ratio**	E (GPa)
345.79	457.39	1.32	0.29	197.056

Note: f_{yb} - characteristic yield strength of the connector (MPa); and f_{em} - characteristic embedment strength of the *Larix gmelinii* (MPa).

Shear connectors used in the current study of high-strength bolts with a diameter of 6 mm and a grade of 6.8. Material tests confirmed their bending yield strength as 425.4 MPa. The bolts were arranged in double rows with spacing of 100 mm (along the span direction). A 10 × 10 mm washer was used to prevent crushing of the timber, and the bolts were tightened by a torque wrench to provide a post-tensioning force of $0.1f_{uf}$, with f_{uf} being the tensile strength of grade 6.8 bolts.

A total of 18 beam specimens were tested in 6 groups as part of the current study. The total length and span of the specimens were 2700 mm and 2520 mm respectively. The cross-section dimensions of glulam slabs in STC beams were 30 × 150 mm, 40 × 150 mm, 50 × 150 mm, 60 × 150 mm, 40 × 100 mm, 40 × 200 mm respectively. It is worth noting that the size of the H Section and the number of shear connectors were the same in all considered specimens. One of the primary objectives of the current study was to investigate the influence of the thickness and width of glulam slabs on the flexural performance of STC beam. Tab. 3 shows the key parameters of specimens of various groups. The variation of mechanical properties and manufacturing methods of glulam will significantly affect the structural properties of STC beams. Therefore, 3 identical specimens were made and tested for each group of STC beams to ensure the accuracy and repeatability of the test results.

Tab. 3: Key parameters of specimens categorized in 6 groups in the current study.

Group N°.	h_1 (mm)	b_1 (mm)	s (mm)	l (mm)	L (mm)	$b \times h$ (mm)
Group A	30	150	100	2520	2700	150×130
Group B	40	150	100	2520	2700	150×140
Group C	50	150	100	2520	2700	150×150
Group D	60	150	100	2520	2700	150×160
Group E	40	100	100	2520	2700	100×140
Group F	40	200	100	2520	2700	200×140

Note: h_1 - thickness of glulam slabs (mm); b_1 - width of glulam slabs (mm); s - spacing of bolts along the span direction (mm); l - span of STC beams (mm); L - length of STC beams (mm); b - width of STC beams (mm); h - height of STC beams (mm)

The test was carried out in accordance with ASTM D198-15 (ASTM D198: 2015). A distribution beam was used to apply symmetrical loads at two sections 420 mm away from the center line of the specimens. Two loading points were equidistant from the support, which was 1/3 of the span of the beams. Supports were placed at each loading point to avoid stress concentration at the loading point and to prevent local crushing of the timber. All testing arrangements are shown in Fig. 2. In order to measure the settlement of the two ends of the beam and to record the deflection at mid-span, two thimble displacement sensors (model: YHD-25, China) were installed at both ends of the supports, designated as LVDT 1 and

LVDT3. One laser displacement sensor (model: KEYENCE IL-300, Japan) was installed under the mid-span of the beams, designated as LVDT 2.

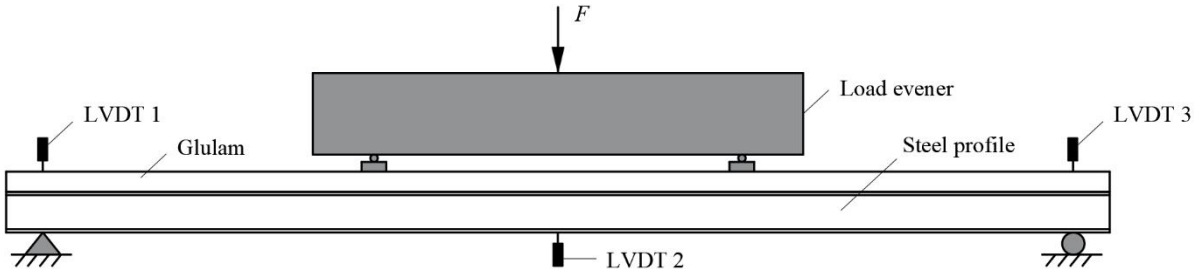

Fig. 2: Set up used for testing STC beams.

Tests were conducted using a microcomputer-controlled electro-hydraulic servo universal testing machine with a capacity of 300 kN and a TDS-530 data acquisition system. The loading regime adopted in the test conforms to ASTM D198-15; the load was applied at a constant rate of 5 $mm \cdot min^{-1}$ until 90% of the ultimate load was reached or some type of damage became obvious.

Finite element model (FEM)

FEM analysis

The FEM of STC beams were established in ABAQUS. Based on the elastoplastic of steel profile and glulam, and the nonlinearity of bolt connection, the numerical simulatio of a four-point bending test was carried out. The STC beam has two symmetrical planes in the four-point bending test. If the out of plane deformation of the steel beam after large deformation was not included (Chybiński and Polus 2019), the model can be treated as a symmetrical model. To reduce the calculation cost, the FEM is 1/4 of the experimental object. In the figure, the red steel plate is the loading steel plate and the support steel plate, the gray part is the glulam beam, the green part is the H-section steel, and the nonlinear element of the simulated bolt connection is located between the glulam and the H-section steel.

The steel profile was simulated by the S4R element, and the shell had 5 integral points along the thickness direction; the glulam was simulated by the C3D8R element. Fig. 3 shows the FE mesh, the element size of the steel profile and glulam was 10 mm, and the mesh size of the loading plate and support plate was larger than that of the steel profile and glulam, which was 25 mm. The vertical interaction between the top surface of the steel profile and the bottom surface of the glulam was simulated by "hard contact", and the tangential action was simulated to Coulomb friction model. The friction coefficient between the steel profile and glulam was set as 0.4. The bolt connection between the steel profile and glulam was simulated by the "connector" in ABAQUS. The nonlinear parameters of the connector were determined by the push-out experimental curves (Yang et al. 2020), and the axial parameters were determined by the axial stiffness of the bolt. The vertical displacement was directly applied on the loading plate to simulate the loading process of bending experiment.

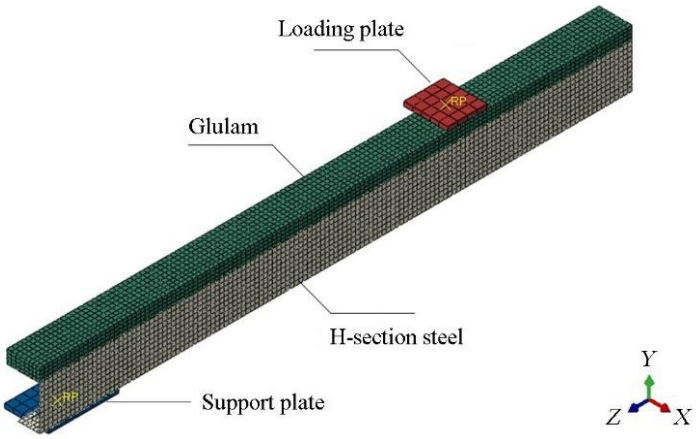

Fig. 3: Mesh grid of FEM.

Constitutive laws of materials

The properties of timber in the FEM were determined by the basic material properties tests. In the bending test of STC beams, the stress characteristics of the upper glulam were mainly the compression along the grain. The timber has better plastic deformation ability under the compression along grain, and the tensile along the grain is brittle failure. For the flexural timber member, because its compression area still has the bearing capacity after exceeding the compression strength, its failure should be limited by its tensile area reaching the tensile strength. In the FE simulation, the ideal elastic-plastic model was used to characterize the compression yield along grain, as shown in Fig. 4. The material properties of steel profile were from the tensile test of the same batch of steel plates. In the FE numerical simulation, the constitutive model of the steel profile was selected as the isotropic trilinear model, as shown in Fig. 5.

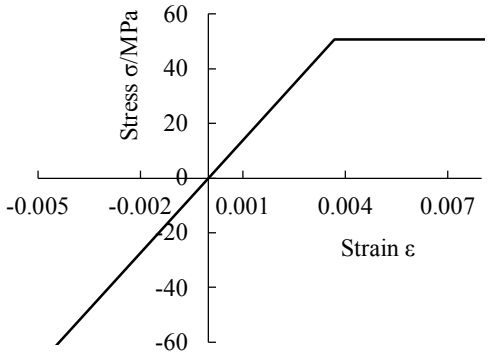

Fig. 4: Elastic-plastic model of timber.

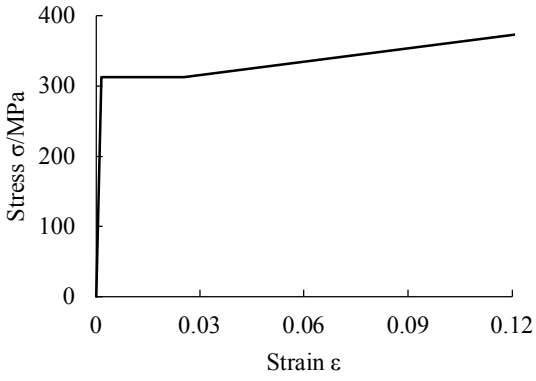

Fig. 5: Trilinear model of steel profile.

Simulation of bolt connection between steel and timber

The H-section steel and glulam in the four-point bending experiment of composite beams were connected by bolts with a diameter of 6 mm. In the FEM, "connector" was used to simulate the tangential and normal mechanical behaviors of bolted connections. The non-linear behavior of the tangent direction of the connector, i.e. the length direction of the STC beam, was determined by the corresponding push-out curves of the glulam with different thickness.

The axial stiffness of the connector was obtained from the conversion of the axial stiffness of the bolt. The position of the connector corresponds to the position of the bolt in the experiment. At the same time, in order to evaluate the influence of the connection between H-section steel and glulam on the mechanical behavior of composite beams, the FEM group of rigid connection was added to compare with the experimental group.

Boundary conditions and loading procedure

The FEM was 1/4 symmetrical for *X* plane and *Z* plane. The symmetrical boundary conditions of *Y*-*Z* plane and *X*-*Y* plane were applied to the symmetrical plane of the *X* plane and *Z* plane respectively. The lower part of the H-section steel was directly placed on the supporting steel plate, and the loading plate of the model was directly placed on the corresponding position of the top surface of the glulam. The contact behavior of loading plate, supporting plate and STC beam was simulated by hard contact, and the tangential behavior was simulated by penalty function. The friction coefficient between the support plate and the lower end of the H-section steel was 0.2, and that between the loading plate and the top of the glulam was 0.4.

The supporting steel plate constrained the translation in the *X* and *Y* directions, released the translation in the *Z* direction, constrained the rotation in the *Y* and *Z* directions, and released the rotation in the *X* direction. The loading steel plate constrained the translation in the *X* direction, and the rotation in the *Y* and *Z* directions, and released the rotation in the *X* direction. The displacement was applied to the loading plate in the *Y* direction (Fig. 6), and was gradually applied to 200 mm in steps of 1 mm.

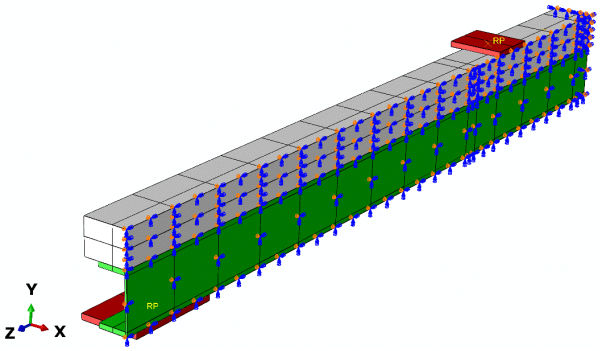

Fig. 6: Boundary condition of FEM.

Validation of FEM

The four-point bending test is a static test, so the solver was selected as the "Static General" in "Standard" during the analysis, regardless of the influence of inertial force. There were 10 groups of FEM. Tab. 4 shows the variable parameter information in each group of models. FE-A to FE-F were the FEM corresponding to the experimental groups; FE-C-150 and FE-C-200 were the FEM with FE-C as the basic model, and bolt spacing changed into 150 mm and 200 mm; FE-SDS was the FEM with self-drilling screw (SDS) as the shear connector; FE-C-Rigid was the rigid connection FEM.

Tab. 4: Summary of FEM information.

Group N°.	h_1 (mm)	b_1 (mm)	Connector type	d (mm)	a_1 (mm)

FE-A	30	150	Bolt	6	100
FE-B	40	150	Bolt	6	100
FE-C	50	150	Bolt	6	100
FE-D	60	150	Bolt	6	100
FE-E	40	100	Bolt	6	100
FE-F	40	200	Bolt	6	100
FE-C-150	50	150	Bolt	6	150
FE-C-200	50	150	Bolt	6	200
FE-SDS	50	150	SDS	5.5	100
FE-C-Rigid	50	150	Rigid connection	-	100

Note: d - nominal diameter of the connector (mm); a_1 - parallel-to-grain connector spacing (mm).

RESULTS AND DISCUSSION

Load-deflection response

Fig. 7 shows the comparison between the FE calculation results of STC beam and the experimental results. Except for the large out of plane deformation in the FE-E, there is deviation between the FE curve and the experimental curves. The change trend of the load-deflection curves of the other FEM is in good agreement with that of the corresponding experimental group. It can be observed that with the increase of the thickness and width of the glulam slab, the difference between the FE group and the experimental group decreases gradually. In the FE-D group, the thickness of glulam slab is the largest, and the difference between the FEM and the experimental results is the smallest, which almost coincides with each other. It is shown that increasing the thickness and width of glulam slab can improve the lateral stiffness of STC beam. Hassanieh et al. (2017) investigated the short-term structural behaviour of STC beams, and they reported the same conclusion. The FEM, selected material parameters and spring element model established in this paper can simulate the bending performance of STC composite beam well. Because the internal defects of the material were not considered in the FEM, the initial stiffness and yield stiffness of the FE curves are slightly higher than the experimental curves. The loading displacement of the FEM is up to 200 mm, while the end displacement of the experimental curves is in the range of 100-150 mm.

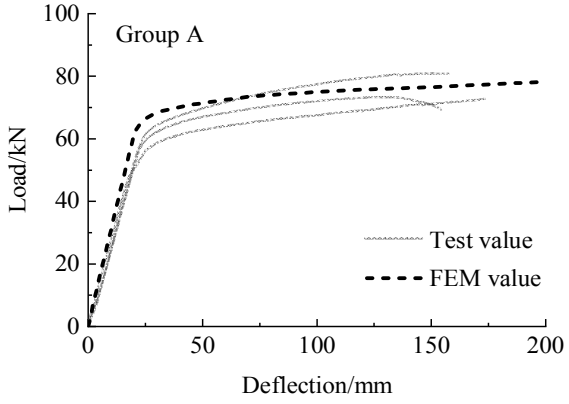

(a) Group A

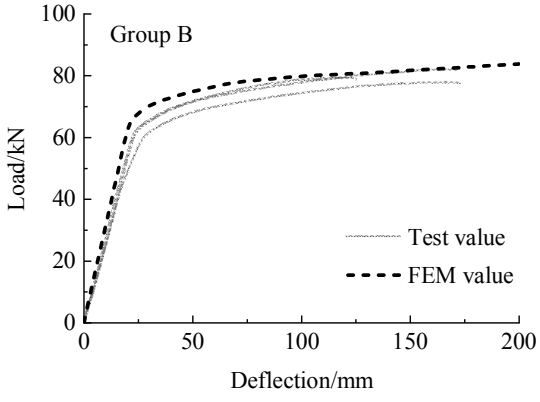

(b) Group B

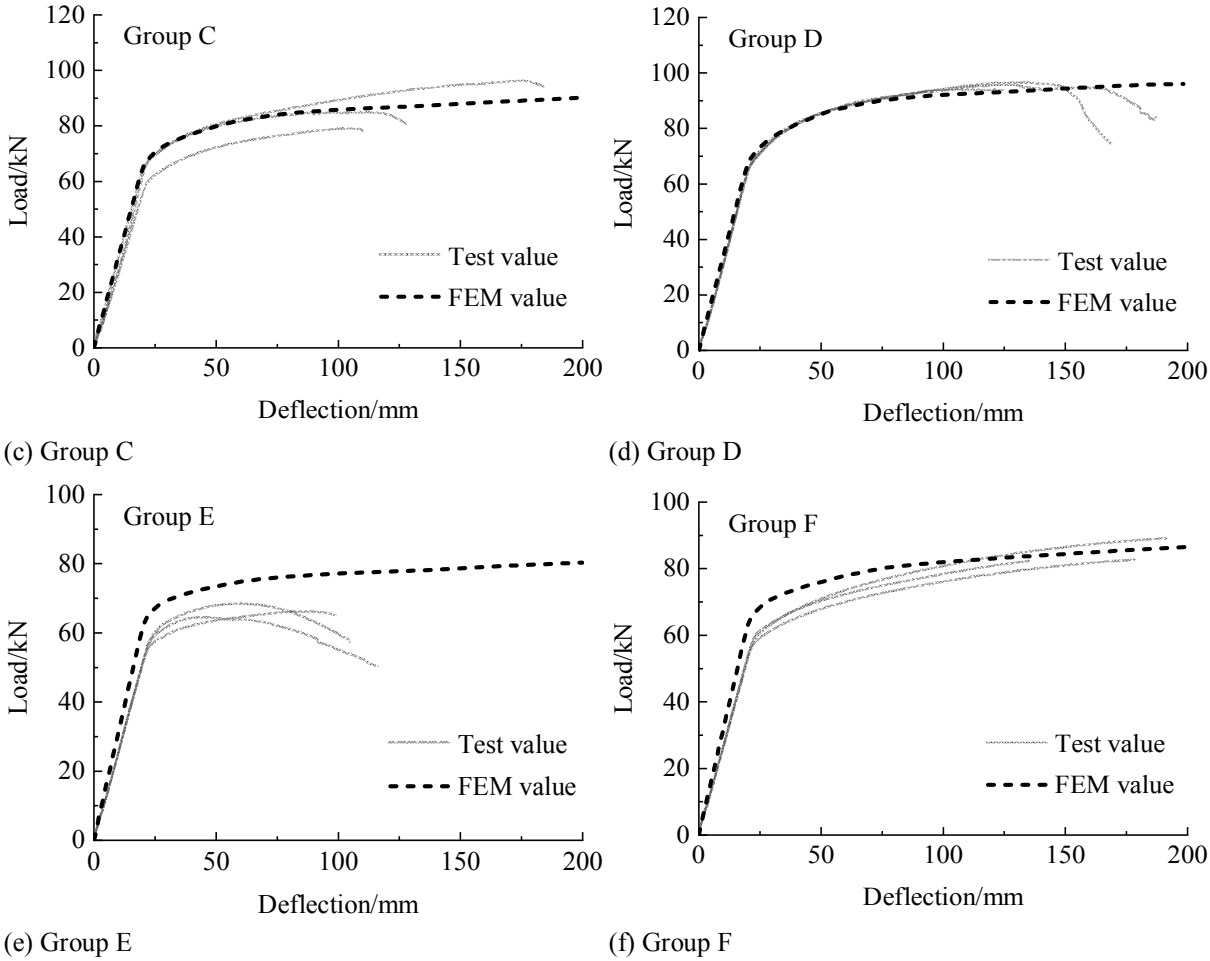

Fig. 7: Comparison between the load-deflection curves of finite element and the experimental.

Tab. 5 shows the comparison between the key points of load-deflection curves of FE-A to FE-D, and the key points of experimental curves. For the yield load, the maximum error between the FE results and the experimental results is 14.85%. The maximum average error of the yield deflection is 12.94%. and of the ultimate load is 16.79%. There are three main reasons for the errors: *(1)* In the FE analysis, 1/4 symmetrical model was selected, the out of plane deformation of STC beams cannot be simulated; *(2)* The defects of the H-section steel and the glulam, the sliding between the loading device and the support at the initial stage of loading were not considered. Therefore, the load-deflection curves of the FEM were generally higher than the experimental curves at the initial stage of loading, and there was no initial sliding phenomenon of the curves. At the later stage of loading, H-section steel and glulam were in the local plastic strengthening stage, and the timber constitutive model used in the FEM cannot accurately simulate the stiffness loss and the complex stress state under the anisotropic condition after the timber enters the strengthening stage; *(3)* At the same time, the nonlinear curves of the bolt connection were different from the load-slip response obtained by the push-out test after the local plastic strengthening stage. Therefore, the ductility and strength of the FEM in the case of large displacement were higher than those of the experimental groups. However, the error of key points was less than 17% (within a reasonable range), which proves that the established finite

element model, selected material parameters and contact element model can better simulate the bending performance of STC beams.

Tab.5: Key points of FEM and test results.

Group	Yield load (kN)		Error (%)	Yield deflection (mm)		Error (%)	Ultimate load (kN)		Error (%)
	Test value	FEM value		Test value	FEM value		Test value	FEM value	
A	56.46	64.84	14.84	21.54	21.03	-2.38	72.85	75.16	3.17
B	58.55	66.72	13.95	22.38	21.24	-5.09	77.81	80.09	2.93
C	65.30	69.84	6.95	21.54	21.29	-1.15	86.61	86.14	-0.54
D	66.61	73.99	11.08	20.30	22.93	12.94	93.92	92.76	-1.24
E	59.68	65.98	10.56	23.49	21.24	-9.59	66.23	77.35	16.79
F	58.71	67.43	14.85	22.37	21.24	-5.04	79.80	82.28	3.11

Note: the ultimate load denotes the load value corresponding to 5 times of the yield deflection. For the test curves, if the 5 times yield deflection exceeds the deflection value corresponding to the peak load, the peak load is used as the ultimate load; Error (%) = [(FEM value − Test value)/ Test value] x 100%.

Development of yield state

The results of FE-D were selected to observe the development of component failure, the stress distribution and plastic yield of H-section steel and glulam with the change of displacement. Fig. 6 shows the experimental and FE results curve of FE-D, in the FE results, 6 points *a*, *b*, *c*, *d*, *e* and *f* were selected, respectively corresponding to the different yield states of the STC beams in the four-point bending experiment. Fig. 7 shows the expansion of yield element of FE-D with displacement.

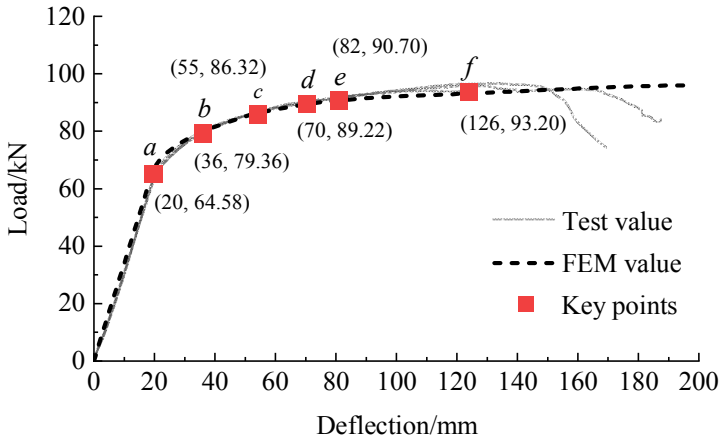

Fig. 6: Key points in the process of stress.

At point "*a*", the deflection is 20 mm, and the load is 64.58 kN. At this time, the material in the bottom flange area of the H-section steel between the loading plates enters the yield state, and the glulam is still in the elastic state; At point "*b*", the deflection is 36 mm, and the load is 79.36 kN. At this time, the yield of the lower flange has developed to the web, and the material yield of the upper flange of the H-section steel appears for the first time, and the glulam is in the elastic state; At point "*c*", the deflection is 55 mm, and the load is 86.32 kN. At this time, the material yield of the lower flange of the H-section steel develops towards the beam length,

the material yield at the web develops along the beam height, and the yield area appears between the loading plates at the top of the glulam for the first time; At point "*d*", the deflection is 70 mm, and the load is 89.22 kN, the yield area of the upper and lower flange of the H-section steel and the web gradually stabilizes, the yield area at the top of the glulam develops towards both sides and depth of the glulam; At point "*e*", the deflection 82 mm, and the load is 90.70 kN, the yield area of the upper flange, lower flange and web of the H-section steel develops slowly, the material yield at the top of the glulam develops along the depth direction, and the material yield area at the bottom of the glulam appears for the first time. At point "*f*", the deflection 126 mm, and the load is 93.20 kN, the yield area of the H-section steel further expands, the yield area between the loading points of the glulam develops along the depth direction, and nearly 60% of the glulam between loading points is in yield state. At this time, it can be seen that most areas of the glulam and H-section between the loading points are in the yield state.

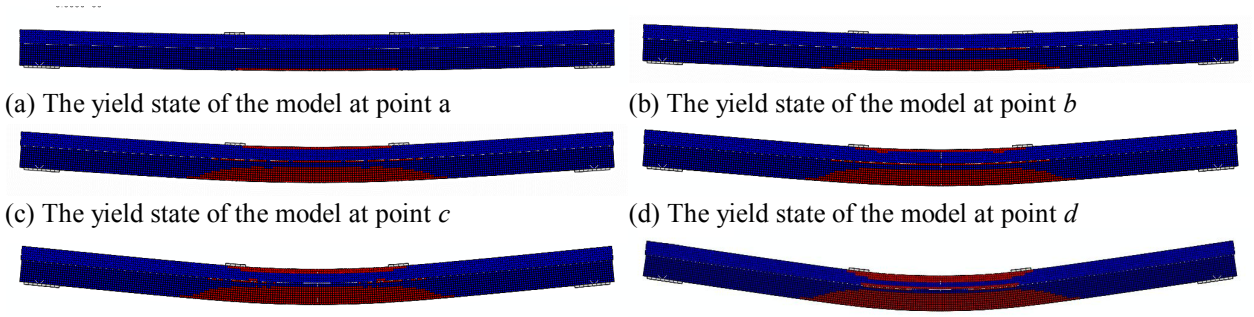

(a) The yield state of the model at point a (b) The yield state of the model at point *b*

(c) The yield state of the model at point *c* (d) The yield state of the model at point *d*

(e) The yield state of the model at point *e* (f) The yield state of the model at point *f*

Fig. 7: Development of yield state for model FE-D during loading.

Parametric study

STC beams involves the combination of two different materials, and its mechanical performance is relatively complex. Many factors will have different degrees of influence on its bending performance. It is not enough to only rely on the long-time and high investment experimental research, and other analysis methods are needed to improve the research accuracy and efficiency. The above has verified the rationality of STC beam FEM. On this basis, the FEM FE-C is selected as the basic model to change the characteristics of shear connector for comparative analysis, to analysis the bending performance of STC beam with these parameters.

In bolt connection, the spacing of bolts was respectively 100 mm, 150 mm and 200 mm. The spacing of the SDS was 100 mm, and the spacing of the rigid connection was 100 mm. The connection properties of bolts with different spacing and SDS were determined by the push-out test (Yang et al. 2020). The rigid connection was realized by setting the tangent and normal attributes of the connector as "Rigid". Tab. 6 shows the FE analysis results of 5 groups of STC beams with different connection characteristics.

As can be seen from Tab. 6, compared with the basic model FE-C, the yield deflection of the rigid connection FEM decreased by -10.85%, the yield load and the ultimate load increased by 12.84% and 6.76% respectively, and the initial stiffness increased by 28.62%; The yield deflection of model FE-SDS decreased by 0.47%, the yield load and the ultimate load increased by 1.09% and 1.29%, and the initial stiffness increased by 3.69%. The yield deflection of

the 150 mm bolt spacing FEM decreased by 1.93%, the yield load and the ultimate load decreased by 0.33% and 1.18%, resp. The yield deflection of the FEM with 200 mm bolt spacing increased by 0.23%, the yield load and the ultimate load decreased by 3.08% and 3.87% resp.

Tab. 6: Key points of FEM with different connections.

Group N°.	ω_y (mm)	Difference (%)	F_y (kN)	Difference (%)	F_u (kN)	Difference (%)	K (kN·mm^{-1})	Difference (%)
FE-C	21.29	-	69.84	-	86.14	-	3.25	-
FE-SDS	21.19	-0.47	70.60	1.09	87.25	1.29	3.37	3.69
FE-C-150	20.88	-1.93	69.61	-0.33	85.12	-1.18	3.29	1.23
FE-C-200	21.34	0.23	67.69	-3.08	82.81	-3.87	3.14	-3.38
FE-C-Rigid	18.98	-10.85	78.81	12.84	91.99	6.79	4.18	28.62

Note: ω_y - yield deflection (mm); F_u - ultimate load, taking the load corresponding to 5 times yield deflection (kN); K - initial stiffness (kN·mm^{-1}); Difference (%) = [(FE value−Experimental value)/ Experimental value] x 100%.

With the increase of bolt spacing, the yield load and the ultimate load decreased, the change of yield deflection was not significant. SDS can increase the yield load and the initial stiffness, but has no significant effect on the yield deflection. The decrease of the yield deflection and the increase of the yield load of the rigid connection are significant. It can be seen that the distribution density and mechanical properties of the connection between the glulam and H-section steel can affect the mechanical behavior of the whole STC beam.

CONCLUSIONS

In current, the finite element (FE) software ABAQUS was used to establish the calculation model and simulate the four-point bending test of steel-timber composite (STC) beams. The results show that the simulated values were in good agreement with the experimental values, and the errors of each key points were in a reasonable range (< 17%). At the same time, the development of yield state and the load-deflection curves of the finite element model (FEM) were in good agreement with the experimental values, which indicates that the established finite element model, the selected material parameters and the contact element models can better simulate the bending performance of STC beams, and provides a FE analysis method for further study of the bending performance of STC beams. Finally, the parametric study was carried out by using the verified FE models, the results show that the distribution density of shear connectors and the mechanical properties of connections can affect the overall mechanical behavior of STC beams. In order to improve the bearing capacity of STC beams in the future, shear connectors with higher stiffness can be considered. At present, the connection form of steel-timber members is still limited, which can be explored and tried in the follow-up research. In addition, the smaller the spacing of connectors, the higher the bearing capacity of STC beams. But in practical application, the utilization rate of materials should also be considered to make the layout of connectors more economical.

ACKNOWLEDGEMENTS

This research is supported by the National First-class Disciplines (PNFD), a Project Funded by the Priority Academic Program Development of Jiangsu Higher Education Institutions (PAPD), and a Project Funded by the Co-Innovation Center of Efficient Processing and Utilization of Forest Resources, Nanjing Forestry University (Nanjing, 210037, China). Any research results expressed in this paper are those of the writer(s) and do not necessarily reflect the views of the foundations. We declare that we do not have any commercial or associative interests, which represent a conflict of interest in connection with the current study.

REFERENCES

1. ANSI A190.1, 2012: Standard for wood products. Structural glued laminated timber.
2. ASTM A370, 2016: Standard test methods and definitions for mechanical testing of steel products.
3. ASTM D143, 2014: Standard test methods for small clear specimens of timber.
4. ASTM D198, 2015: Standard test methods of static tests of lumber in structural sizes.
5. Chybiński, M., Polus, Ł., 2019: Theoretical, experimental and numerical study of aluminium-timber composite beams with screwed connections. Construction and Building Materials 226(30): 317-330.
6. Daňková, J., Mec, P., Šafrata, J., 2019: Experimental investigation and performance of timber-concrete composite floor structure with non-metallic connection system. Engineering Structures 193: 207-218.
7. Deam, B.L., Fragiacomo, M., Buchanan, A.H., 2008: Connections for composite concrete slab and LVL flooring systems. Materials and Structures 41(3): 495-507.
8. Fojtik, R., Kubincova, L., Dubovsky, V., Kozlova, K., 2020: Moisture at contacts of timber-concrete element. Wood Research 65(6): 917-924.
9. GB 50011, 2016: Code for seismic design of buildings. Beijing (in Chinese).
10. GB 50017, 2017: Code for design of steel structure. Beijing (in Chinese).
11. Hassanieh, A., Valipour, H.R., Bradford, M.A., 2016: Experimental and numerical study of steel-timber composite (STC) beams. Journal of Constructional Steel Research 122: 367-378.
12. Hassanieh, A., Valipour, H.R., Bradford, M.A., Sandhaas, C., 2017: Modelling of steel-timber composite connections: Validation of finite element model and parametric study. Engineering Structures 138: 35-49.
13. Hassanieh, A., Valipour, H.R., Bradford, M.A., 2018: Bolt shear connectors in grout pockets: Finite element modelling and parametric study. Construction and Building Materials 176: 179-192.
14. Jorge, L.F.C., Lopes, S.M.R., Cruz, H.M.P., 2011: Interlayer influence on timber-LWAC composite structures with screw connections. Journal of Structural Engineering 137: 618-624.

15. Khorsandnia, N., Valipour, H.R., Crews, K., 2012: Experimental and analytical investigation of short-term behaviour of LVL-concrete composite connections and beams. Construction and Building Materials 37: 229-238.
16. Leborgne, M.R., Gutkowski, R.M., 2010: Effects of various admixtures and shear keys in wood–concrete composite beams. Construction and Building Materials 24(9): 1730-1738.
17. Li, H.T., Wu, G., Zhang, Q.S., Deeks, A., Su, J.W., 2017: Ultimate bending capacity evaluation of laminated bamboo lumber beams. Construction and Building Materials 160: 365-375.
18. Li, Q., Wang, Z.Q., Liang, Z.J., Li, L., Gong, M., Zhou, J.H, 2020: Shear properties of hybrid CLT fabricated with lumber and OSB. Construction and Building Materials 261: 120504.
19. Liu, X.P., Bradford, M., Chen, Q.J., Ban, H., 2016: Finite element modelling of steel–concrete composite beams with high-strength friction-grip bolt shear connectors. Finite Elements in Analysis and Design 108: 54-65.
20. Naud, N., Sorelli, L., Salenikovich, A., Auclair, S.C, 2019: Fostering GLULAM UHPFRC composite structures for multi-storey buildings. Engineering Structures 188: 406-417.
21. Nouri, F., Valipour, H.R., Braford, M.A., 2019: Structural behaviour of steel-timber composite (STC) beam-to-column connections with double angle web cleats subjected to hogging bending moment. Engineering Structures 192: 1-17.
22. Nouri, F., Valipour, H.R., Braford, M.A., 2019: Finite element modelling of steel-timber composite beam-to-column joints with nominally pinned connections. Engineering Structures 201: 109854.
23. Pulngern, T., Chanto, K., Pansuwan, W., Pattaraumpornsak, W., 2020: Effect of lamina thickness on flexural performance and creep behavior of douglas fir glued laminated timber beam. Wood Research 65(5): 715-726.
24. Schänzlin, J., Fragiacomo, M., 2018: Analytical derivation of the effective creep coefficients for timber-concrete composite structures. Engineering Structures 172: 432-439.
25. Xu, B.H., Bouchaïr, A., Racher, P., 2015: Mechanical behavior and modeling of dowelled steel-to-timber moment-resisting connections. Journal of Structural Engineering 141(6): 04014165.
26. Yang, R.Y., Li, H.T., Lorenzo, R., et al, 2020: Mechanical behaviour of steel timber composite shear connections. Construction and Building Materials 258: 119605.
27. Yang, R.Y., Zhang, X.F., Sun, Y.F., Zhou, T.T, Yuan, Q., 2020: Effect of the metallization treatment on the surface properties of *Populus Euphratica*. Wood Research 65(3): 381-394.
28. Yeoh, D., Fragiacomo, M., Franceschi, M.D., Heng, B.K., 2011: State of the art on timber-concrete composite structures: literature review. Journal of Structural Engineering 137(10): 1085-1095.

RUYUAN YANG*
NANJING TECH UNIVERSITY
COLLEGE OF ART & DESIGN
NANJING, CHINA

JIA WAN
TAIYUAN UNIVERSITY OF TECHNOLOGY
COLLEGE OF CIVIL ENGINEERING
TAIYUAN, CHINA

XIAOFENG ZHANG, YOUFU SUN
NANJING FORESTRY UNIVERSITY
COLLEGE OF MATERIALS SCIENCE AND ENGINEERING
NANJING, CHINA
*Corresponding author: ryyang0404@163.com